Ramp sampling and projection reconstruction

Charles L. Epstein and Jeremy Magland*

LSNI, Department of Radiology, HUP

and

Department of Mathematics, University of Pennsylvania

Version 2.0 December 27, 2004

*Corresponding author: CL Epstein, address: Department of Mathematics, 209 S. 33rd Street, Philadelphia, PA. 19104-6395; e-mail: cle@math.upenn.edu

Abstract

When imaging objects with a very short T_2 it is often useful to collect samples of the Fourier transform of the spin density as the gradient is ramping up to its steady state value. This leads to a collection of samples that are not uniformly spaced in k-space. It is shown how, using a simple algorithm, one can exactly recover the missing uniformly spaced samples. This algorithm is called *exact uniform sample recovery* or *EUSR*. A consequence of the derivation of the EUSR method is that *any* simple interpolation technique introduces errors into the measurements. In examples it is shown that this leads to non-localized artifacts in images reconstructed using filtered backprojection. Comparisons are also made with an algorithm that uses the non-uniformly spaced samples directly.

Keywords: ramp sampling, interpolation, non-uniform spacing, exact uniform sample recovery, EUSR

1 Introduction

When imaging very short T_2-species, it is useful to be able to begin acquiring a signal as soon after the RF-excitation as possible. One way to shorten the acquisition time is to skip the phase encoding step and begin sampling as soon as the excitation is rephased. This entails collecting samples on the rising portion of the gradient ramp. If $\rho(x, y)$ is the spin density in the excited slice, then (ignoring relaxation) the signal, as a function of time, is given by

$$S(t) = e^{i\omega_0 t} \int_{\mathbb{R}^2} \rho(x, y) e^{ik(t)\langle (x,y), \boldsymbol{w}_\theta \rangle} dx dy. \tag{1}$$

Here $\boldsymbol{w}_\theta = (\cos\theta, \sin\theta)$, the time parameter t is normalized so that the excitation is rephased at $t = 0$, and

$$k(t) = \gamma \int_0^t g(s) ds. \tag{2}$$

The strength of the gradient, as a function of (x, y) and t, is given by $g(t)\langle (x, y), \boldsymbol{w}_\theta \rangle$. Let $R\rho(s, \theta)$ denote the Radon transform of ρ, see [1]. If ρ is supported in the disk of radius L centered at 0, then, the central slice theorem implies that the integral in equation (1) can be re-expressed as

$$S(t) = e^{i\omega_0 t} \int_{-L}^{L} R\rho(s, \theta) e^{ik(t)s} ds, \tag{3}$$

see [1]. Below we let $\widetilde{R}\rho(k, \theta)$ denote the 1-dimensional Fourier transform of $R\rho(s, \theta)$ in the s-variable.

In this context it makes sense to sample k-space on a set of uniformly spaced rays passing through 0, i.e. $\theta_l \in \{p\Delta\theta : \ p = 0, \ldots, P\}$. One can then reconstruct the image using a filtered backprojection algorithm, see [1]. Due to hardware limitations, data is usually collected by sampling $S(t)$ at a set of uniformly spaced times $\{j\Delta t : \ j = 0, \ldots, N\}$. As noted above, the function $g(t)$ is increasing for $t \in [0, t_0]$ and is a constant, g_0, for the remainder of the acquisition period, $[t_0, t_1]$. If M denotes the greatest integer in $t_0/\Delta t$, then the samples

$$a_j = S(j\Delta t), \quad j = 0, \ldots, M, \tag{4}$$

are obtained at the *unequally* spaced frequencies:

$$k_j = k(j\Delta t). \tag{5}$$

The samples,

$$b_j = S(j\Delta t), \quad j = M+1, \ldots, N, \tag{6}$$

are measured at the equally spaced frequencies $\{k(j\Delta t) : \ j = M+1, \ldots, N\}$. The spacing for the uniformly spaced samples is $\Delta k = \gamma g_0 \Delta t$.

We assume that the ramp and sample spacing are selected so that, for some integer l_0, we have the relation

$$k((M+1)\Delta t) = l_0 \Delta k. \tag{7}$$

These assumptions imply that we measure the non-uniformly spaced samples,

$$\{\widetilde{R}\rho(k_j, \theta_l) : \ j = 0, \ldots, M\} \tag{8}$$

and uniformly spaced samples

$$\{\widetilde{R}\rho(j\Delta k, \theta_l) : \ j = l_0, \ldots, l_0 + N - M + 1\}. \tag{9}$$

Note that in general $l_0 < M + 1$, so that the low frequencies are, in some sense, oversampled. In general $\widetilde{R}\rho(-k, \theta) = \widetilde{R}\rho(k, \theta + \pi)$, hence the measurements at $\theta_l + \pi$ can be used to determine

$$\{\widetilde{R}\rho(-k_j, \theta_l) : \ j = 0, \ldots, M\} \tag{10}$$

and

$$\{\widetilde{R}\rho(-j\Delta k, \theta_l) : \ j = l_0, \ldots, l_0 + N - M + 1\}. \tag{11}$$

We call the samples in equations (8) and (10) the "low frequency samples," and the samples in equations (9) and (11) the "high frequency samples." For this application, a similar analysis applies if

$$k((M + 1)\Delta t) = (l_0 + \frac{1}{2})\Delta k.$$

In order to use filtered backprojection it would be very useful to determine the "missing" uniformly spaced samples, $\{\widetilde{R}\rho(j\Delta k, \theta_l) : \ j = 1 - l_0, \ldots, l_0 - 1\}$. The standard approach would be to use the measurements $\{a_0, \ldots, a_M\}$ to interpolate values for these samples. In the next section we derive an exact expression for the missing samples in terms of these samples *as well as* the high frequency samples. We call this approach *EUSR*, for *example uniform sample recovery*. This formula

shows that using any interpolation method introduces errors in the values of the low frequency Fourier coefficients. In the final section we give examples that show how these interpolation errors produce non-localized artifacts in the reconstructed images. We also compare with reconstructions obtained using a method that uses the non-uniformly spaced data directly. In real applications, such a method would be implemented using a gridding method. For reasons explained in Section 3, we compute the required trigonometric sums directly. In these examples we see that subtle details of the time course of the gradient can have a noticeable effect on an image reconstructed using a direct method, whereas it has no effect on the image obtained using FBP with EUSR.

2 Theory

In this section we consider the problem of determining the missing uniformly spaced samples of the Fourier transform of a function $f(s)$. In applications to MRI one can take $f(s) = R\rho(s, \theta_l)$. We assume that the support of $f(s)$ is contained in the interval $[-L, L]$, and denote the Fourier coefficients of $f(s)$ by

$$b_n = \int_{-L}^{L} f(s) e^{-i\frac{\pi n s}{L}} ds. \tag{12}$$

Motivated by the discussion above, we assume that the following non-uniformly spaced low frequency samples of the Fourier transform of f are available:

$$a_j = \int_{-L}^{L} f(s) e^{-i\frac{\pi k_j s}{L}} ds,\ j = -M, \ldots, M \tag{13}$$

as well as the uniformly spaced high frequency samples $\{b_n : |n| \geq l_0\}$. Here $\{k_{-M}, \ldots k_M\}$ are distinct numbers between $-l_0$ and l_0.

Because $f(s)$ is supported in $[-L, L]$ we can express it in terms of a Fourier series

$$f(s) = \frac{1}{2L} \sum_{n=-\infty}^{\infty} b_n e^{i\frac{\pi n s}{L}}, \qquad \text{for } s \in [-L, L]. \tag{14}$$

This expression can be substituted into equation (13) to obtain the relations

$$a_j = \sum_{n=-\infty}^{\infty} A_{jn} b_n, \tag{15}$$

where

$$\begin{aligned} A_{jn} &= \frac{1}{2L} \int_{-L}^{L} e^{i\frac{s\pi(n-k_j)}{L}} ds \\ &= \operatorname{sinc}(\pi(n - k_j)). \end{aligned} \tag{16}$$

This is just the usual "sinc"-interpolation formula, expressing $\{\hat{f}(k_j)\}$ in term of the uniformly spaced samples of $\hat{f}$. But in the present circumstance, we have measured $\{\hat{f}(k_j)\}$ and so we rewrite the expression in equation (15) to obtain

$$\sum_{n=1-l_0}^{l_0-1} A_{jn} b_n = a_j - \sum_{|n|\geq l_0} A_{jn} b_n, \quad j = -M, \ldots, M. \tag{17}$$

Note that everything on the right hand side is assumed known, and, therefore this is a system of $2M + 1$-equations for the $2l_0 - 1$ unknown samples $\boldsymbol{b}' = (b_{1-l_0}, \ldots, b_{l_0-1})$.

As noted above, in most applications, $l_0 < M$ so this is an overdetermined system. For most choices of frequencies $\{k_{-M}, \ldots, k_M\}$ the matrix

$$A' = \left(A_{jn}\right)_{j=-M,|n|<l_0}^{j=M}$$

has rank $2l_0 - 1$ and hence, there is a unique least squares solution for $\boldsymbol{b}'$. For most choices of frequencies $\{k_j\}$ the matrix

$$A'' = \left(A_{jn}\right)_{j=-M,|n|\geq l_0}^{j=M}$$

is nonzero. Hence equation (17) implies that $\boldsymbol{b}'$ is *not* determined by the low frequency measurements $\boldsymbol{a} = (a_{-M}, \ldots, a_M)$. Note also that with perfect measurements, the system of equations in (17) has a unique solution and therefore the residual error provides a measure of the quality of the data.

In real applications, the values $\{b_n\}$ are known for a finite collection of indices. These Fourier coefficients and the matrix elements A_{jn} decay as n tends to infinity, and so, with adequate sampling, this does not lead to difficulties in practice. If $\boldsymbol{b}''$ denotes the uniformly spaced high frequency samples, then the system of equations can be concisely rewritten as

$$A'\boldsymbol{b}' = \boldsymbol{a} - A''\boldsymbol{b}''. \tag{18}$$

Provided A' has maximal rank, the least squares solution is given by

$$\boldsymbol{b}' = [A'^{t} A']^{-1} A'^{t} (\boldsymbol{a} - A''\boldsymbol{b}''). \tag{19}$$

3 Methods and Results

In this section we compare various reconstruction methods with non-uniformly sampled projection data. We examine the consequences of filling in the missing uniformly spaced samples using a spline interpolation algorithm versus the EUSR method. We also compare to an algorithm that directly uses the non-uniformly spaced frequency information. In a real application, a method of this sort would be implemented using a "gridding" algorithm [3]. Gridding algorithms are nothing more nor less than fast algorithms for computing exponential sums with non-uniformly spaced frequencies, see [2]. In the sequel, we refer to these examples as being computed using a "direct method." These images could have been obtained using a gridding method, but this would only introduce a further source of error.

An essential part of any algorithm that directly uses non-uniformly spaced samples is the choice of weight factors, or density compensation factors. For our examples we use the so-called "Voronoi weights." This is a standard choice that arises from the interpretation of these sums as Riemann sums for one dimensional Fourier

integrals,

$$\begin{aligned} f(s) &= \frac{1}{2\pi} \int_{-\infty}^{\infty} \hat{f}(k) e^{iks} dk \\ &\approx \sum_{j=-N}^{N} \hat{f}(k_j) e^{ik_j s} w_j . \end{aligned} \tag{20}$$

If $\{k_j\}$ are the frequencies, then the Voronoi weight assigned to the frequency k_j is

$$w_j = \frac{k_{j+1} - k_{j-1}}{2}. \tag{21}$$

Geometrically, this is the length of the interval consisting of points closer to k_j than any other sample frequency. There are methods for selecting weights that produce more accurate reconstructions, but only with a concommitent loss in the size of the field-of-view. A discussion of the problem of choosing weights is beyond the scope of this article.

For these numerical experiments, $\rho(x, y)$ is defined using the modified Shepp-Logan head phantom provided by Matlab. The range of densities in this image is quite similar to that found in actual MR data sets. We use a 1024×1024-phantom and sample the Radon transform, $R\rho(s, \theta)$ at 720 angles. For the reconstructions done with uniformly spaced samples, we use 703 uniformly spaced frequencies. All the data sets have the same maximum frequency and hence all the images have the same intrinsic resolution.

When using different reconstruction algorithms, it is very difficult to control the exact spatial grid on which the images are reconstructed. In order to compare

the images obtained using different approaches, it is useful to be able to compute difference images. To control the reconstruction grid sufficiently well for the difference images to reflect the differences in the algorithms and not merely small differences in the reconstruction grid, we have employed the following artifice: The "measured" Fourier projection data, $\{\widetilde{R}\rho(k_j, \theta_l)\}$ is used to reconstruct evenly spaced samples of the Radon transform $\{R\rho(md, \theta_l)\}$. The images are then reconstructed on a fixed grid using the Matlab routine "iradon." The different ways of using the frequency data are captured by different approaches to computing $\{R\rho(md, \theta_l)\}$:

1. Using spline interpolation we first approximate uniformly spaced samples of $\widetilde{R}\rho(k, \theta_l)$. The samples, $\{R\rho(md, \theta_l)\}$ are then found using a uniformly spaced inverse Fourier transform.

2. Using EUSR we find the missing uniformly spaced samples of $\widetilde{R}\rho(k, \theta_l)$. The samples, $\{R\rho(md, \theta_l)\}$ are found using a uniformly spaced inverse Fourier transform.

3. Using sums like those in the second line of equation (20), with weights given in equation (21), we use $\{\widetilde{R}\rho(k_j, \theta_l)\}$ to directly compute approximations to the samples $\{R\rho(md, \theta_l)\}$.

This approach allows us to model the effects of the different reconstruction algo-

rithms and obtain meaningful difference images. As the difficulties of using non-uniformly spaced samples increase with the dimension, the accuracy of a standard 2d-gridding algorithm, using the non-uniformly spaced samples, is unlikely to be better than (or even as good as) the accuracy of the approach we have followed. The artifacts seen in the examples below are similar in appearance and magnitude to those we have seen in reconstructions that use a standard 2d-gridding algorithm with Voronoi weights.

***Example* 1.** In the first set of figures we use 41 non-uniformly spaced samples. This means that, in equation (7), $M = 20$ and $l_0 = 10$. In our first experiment the non-uniformly spaced samples are linearly spaced, as would be the case with a trapezoidally shaped gradient profile. The sample spacings for the non-uniformly spaced samples are

$$\begin{aligned} &0.0476, 0.0952, 0.1429, 0.1905, 0.2381, 0.2857, 0.3333, \\ &0.3810, 0.42860.4762, 0.5238, 0.5714, 0.6190, 0.6667, 0.7143, 0.7619, \\ &0.8095, 0.8571, 0.9048, 0.9524, 1.0000, \ldots \end{aligned} \tag{22}$$

Notice that the sample spacing is monotonically increasing.

Figure 1(a) shows a reconstruction of the phantom with uniformly samples of $\widetilde{R}\rho(k, \theta)$. Using a inverse Fourier transform, this data is used to compute samples of $R\rho(s, \theta)$. The image is reconstructed using iradon; this is our "reference" figure. The other images are difference images. Figure 1(b) is the difference of (a) and the

image obtained using EUSR; Figure 1(c) is the difference of (a) and the image obtained using spline interpolation; Figure 1(d) is the difference of (a) and the image obtained using a direct algorithm. These images are unwindowed.

The maximum pixel value in Figure 1(a) is about 5. The maximum error in the EUSR image is about 3×10^{-7}, in the spline image it is about 1.5×10^{-2}, and in the direct image about 3×10^{-2}. The direct reconstruction can be improved by using a more sophisticated algorithm to choose the weights. As noted above, this leads to a reduction in the field-of-view in the sense that "optimal" weights produce smaller errors near the center of the field-of-view and much larger errors near the edge. The errors produced by the optimal weights are still several orders of magnitude larger than those produced by EUSR. This will be the subject of a subsequent publication.

Using cubic spline interpolation and the FBP gives a reasonably good image, though with a non-localized oscillatory artifact. The generally good quality of this image is not surprising as the Fourier transform, $\hat{f}(k)$, of a function, $f(t)$, with bounded support, is smooth. The derivatives of $\hat{f}$ are given by

$$\partial_k^j \hat{f}(k) = (ik)^j \hat{f}(k).$$

Hence, all the derivatives of $\hat{f}$ are small for low frequencies. It therefore stands to reason that a high order interpolation method, whose error is proportional to $h^2 \partial_k^2 \hat{f}$, here h is the "mesh size", should give good results for low frequencies. On

the other hand, using linear interpolation produces a terrible image. As explained in the previous section, any interpolation method produces somewhat incorrect values for the low frequency samples. This explains the oscillatory artifact in Figure 1(c) whose radial frequency is roughly the frequency of the first uniformly spaced sample that is collected.

The computations were performed on a 2GHz Linux box using standard Matlab functions. As we are constrained by the need to produce all images on a single reconstruction grid, no attempt was made to compare the speeds of the different algorithms. Since the same non-uniformly spaced frequencies are used for every ray, the EUSR step requires a modest amount of computation time.

***Example* 2.** In the second set of examples we consider the effect of a small overshoot in the gradient before it settles down to its constant equilibrium value. This leads to a non-uniform sample spacing that is not monotonic. We have simulated a 4%, and 10% overshoot. The sample spacings are those given in (22) with two additional samples. We list the last few non-uniform sample spacings:

$$\begin{aligned} &\text{4\% overshoot: } 0.9048, 0.9524, 1.0000, 1.0400, 0.9600, 1.0000, \ldots \\ &\text{10\% overshoot: } 0.9048, 0.9524, 1.0000, 1.1000, 0.9000, 1.0000, \ldots \end{aligned} \tag{23}$$

The non-monotonicity of the sample spacing has no effect on the FBP with EUSR, however it produces a noticeable change in the direct reconstructions. As before, the magnitude of this artifact can be reduced by choosing different weights,

but, as noted above, this also reduces the useful field of view. In Figure 2 we show the differences between the images produced with the direct algorithm and the reference image from Figure 1(a).

***Example* 3.** As a final example we consider the effects of noise on the EUSR algorithm. If the noise in the two images is not "identical," then the difference image is overwhelmed by the noise. In order to get images that can be compared, we add (pseudorandom) noise to the phantom before we compute the Fourier transform data $\{\widetilde{R}\rho(k_j, \theta_l)\}$, rather than adding noise directly to the k-space data. Figure 3 is the difference between the uniformly spaced image reconstructed from nosiy data and that produced by EUSR using the same noisy image and the non-uniformly spaced frequencies from Example 1. The additive noise is adjusted so that the per-pixel noise in the reconstructed image is about 0.5, which is much worse than in typical MR applications. The maximum error, $\pm 8 \times 10^{-6}$, in the image reconstructed using EUSR is still quite small, though it is 20-times as large as that for the noise-free data. This increase in the error is probably due to the truncation of the sum over n in equation (17), and the fact that the power spectrum of noise is nearly flat. Although the noise in this illustration does not exactly represent the kind of noise encountered in an MR experiment, the results suggest that the EUSR algorithm is not especially sensitive to noise in the data.

4 Discussion

We present a simple algorithm (EUSR) for recovering uniformly spaced low frequency samples of the Fourier transform of a function from non-uniformly spaced low frequency samples and uniformly spaced high frequency samples. Since the EUSR algorithm involves only the 1-dimensional Fourier transform and, implicitly the central slice theorem, this approach applies equally well to direct 3d projection imaging. It can also be parallelized. The derivation of the algorithm shows that any interpolation method introduces errors. In examples we show that, when spline interpolation is used with the filtered backprojection algorithm, it leads to a global artifact in the reconstructed image.

The errors produced by the EUSR algorithm are almost 5 decimal orders of magnitude smaller than those produced using either spline interpolation or a direct method. The errors produced using a direct method can be reduced by using "optimal" weights, but this has the side effect of diminishing the useful field of view. The range of the errors shown in Figure 2(a) is about twice that shown in Figure 1(a) and that in Figure 2(b) about four times. The EUSR algorithm is also shown to be rather tolerant of noise in the data.

Acknowledgments

Research of both authors partially supported by NSF grant DMS02–03705.

Dr. Magland's research partially supported by NIH traning grant in quantitative MRI. We would like to thank Felix Wehrli and Sailaja S. Anumula for bringing this problem to our attention and Hee Kwon Song for useful remarks. We would also like to thank the referees for several useful suggestions.

5 Figures

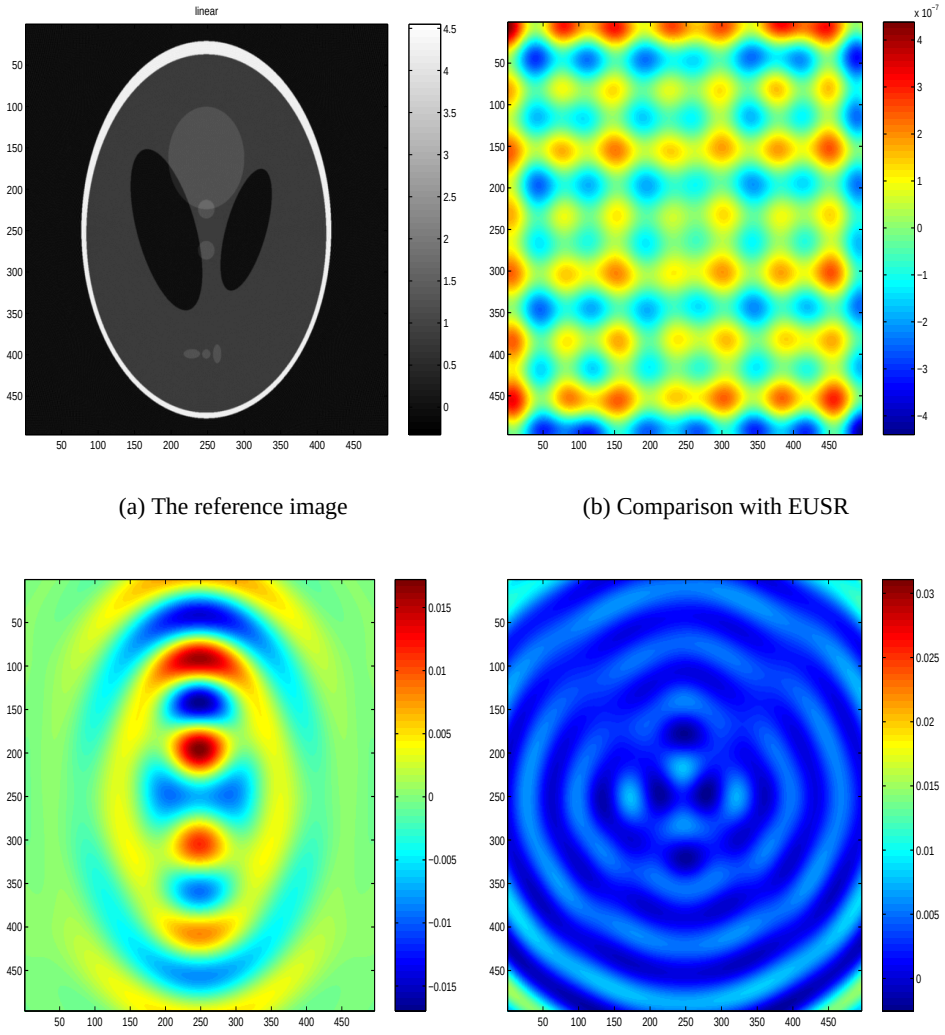

(a) The reference image

(b) Comparison with EUSR

(c) Comparison with spline

(d) Comparison with the direct method

Figure 1. Comparison of reconstructions obtained using different reconstruction algorithms. Figure (a) shows the reference image, reconstructed using 720 views and 703 uniformly spaced frequencies. Figures (b-d) are difference images between Figure (a) and the images reconstructed using the indicated methods, employing non-uniformly spaced samples. These figures use 41 non-uniformly spaced samples. Note the different scales shown on the color bars.

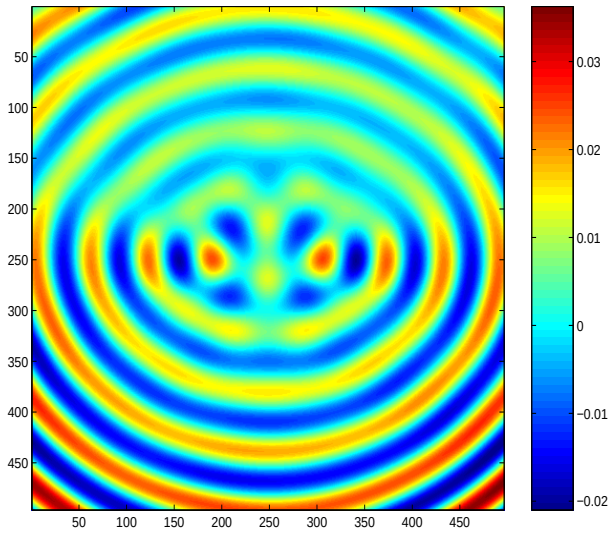

(a) 4%-overshoot

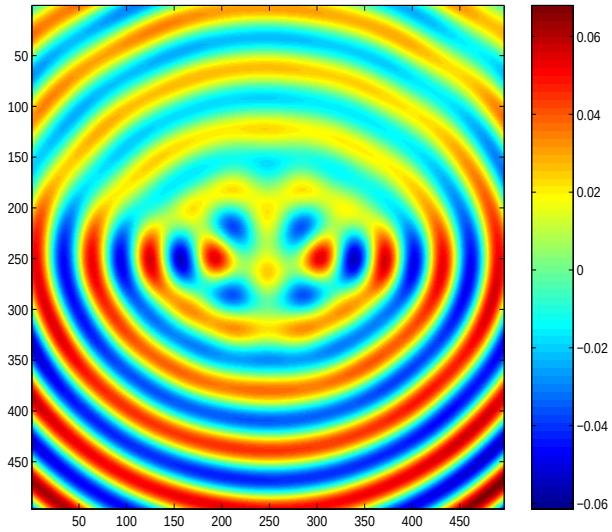

(b) 10%-overshoot

Figure 2. Differences between the reference figure, Figure 1(a) and images constructed using the direct method. These figures show the effects of non-monotonicity in the sample spacing on reconstructions that directly use the non-uniformly spaced samples.

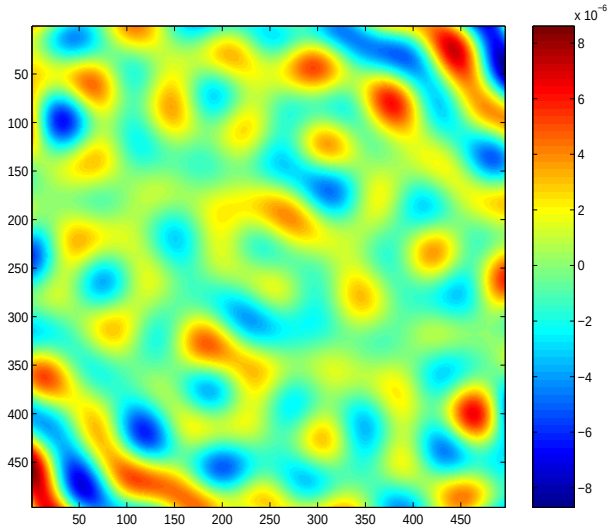

Figure 3. Comparison of EUSR and uniformly spaced sampling acting on an image with additive noise leading to a per-pixel SNR of about 0.5.

References

[1] C. L. EPSTEIN, *Introduction to the Mathematics of Medical Imaging*, Prentice Hall, Upper Saddle River, NJ, 2003.

[2] L. GREENGARD AND J.-Y. LEE, *Accelerating the nonuniform fast Fourier transform*, SIAM Review, 46 (2004), pp. 443–454.

[3] J. O'SULLIVAN, *A fast sinc function gridding algorithm for Fourier inversion in computed tomography*, IEEE Trans. in Med. Imag., 4 (1985), pp. 200–207.